Research Article Vol. 34, No. 8 / 20 Apr 2026 / Optics Express 13788
Optics EXPRESS

Analytic model for the autocorrelation matrix based on piecewise-functional spectra, and its application in camera characterization

D. Andrew Rowlands[1,2,3,4] and Graham D. Finlayson[1]

[1]Colour & Imaging Lab, School of Computing Sciences, University of East Anglia, Norwich NR4 7TJ, United Kingdom
[2]Sino-British College, University of Shanghai for Science & Technology, Shanghai 200093, China
[3]d.a.rowlands@uea.ac.uk
[4]andy.rowlands@sbc.usst.edu.cn

Abstract: The concept of piecewise-functional spectra is introduced as a tool for modeling autocorrelation statistics in the context of reflectance and color-signal spectra. By considering an infinite set of such spectra that satisfy any target statistics, a closed-form expression is obtained for the autocorrelation matrix. Significantly, the model only contains a single tuning parameter that enables the degree of correlation to be adjusted. Interestingly, if the autocorrelation statistics do not vary as a function of wavelength, then the model spectra become piecewise constant. The utility of the idea is demonstrated in the context of camera color characterization. Here a model of the reflectance spectra can be exactly characterized, which is important because it is not possible to measure or numerically calculate all reflectances that might be encountered in the real world.

1. Introduction

Many color and image processing algorithms are trained using a set of reflectance, illumination, or color-signal spectra. Typically, such datasets are relatively small, ranging from the few chips available on a color-checker chart to a few thousand real-world measured spectra, e.g. [1–5]. However, the ranking of algorithms in terms of performance can change depending on the dataset used [6]. Although measured datasets can be ideal for controlled applications, for example the rendering of skin color under studio lighting, spectra in the real world often mix together and a device such as a camera may record any convex mixture of measured spectra [6]. Mathematically, taking all mixtures means all convex combinations, which rapidly becomes intractable [6,7].

As a way forward, let us consider piecewise functions, which have a long history in mathematics and science. In the context of color, Schrödinger's optimal object colors [8] are based upon binary piecewise-constant reflectance spectra, and more recently Logvinenko used a specific type of piecewise-constant function to model metameric reflectance spectra [9]. In this paper, the concept of piecewise-functional (PF) spectra is introduced, and such spectra can be randomly generated according to a desired statistical model. For example, the mean and standard deviation can be varied as a function of wavelength. Significantly, the model uses a single parameter, α, to control the degree of correlation between the spectra, which can also be varied as a function of wavelength if required. An important property of the construction is that an infinite set of such spectra can be analytically integrated over to obtain a closed-form solution for the associated autocorrelation matrix, which is central to a variety of color and image processing algorithms, e.g. [10–12].

#579609 https://doi.org/10.1364/OE.579609
Journal © 2026 Received 19 Sep 2025; revised 27 Jan 2026; accepted 9 Feb 2026; published 7 Apr 2026

Optics EXPRESS

An important application is camera characterization, also referred to as color correction, where the reflectance autocorrelation matrix is the central object of interest. For a camera to be colorimetric, its spectral responsivities must be a perfect linear combination of the human eye response functions, which is known as the Luther-Ives condition [13]. In general, this condition is not satisfied, however the color error can be minimized. Although camera characterization methods remain an active area of research [14–17], the fundamental method for transforming from the linear camera raw space to the CIE XYZ reference color space is a 3×3 linear matrix transform based upon least-squares regression [17–19]. There are two main approaches to determining the matrix transform, both of which are described in the ISO 17321 standard [12]. One approach is to photograph a color-checker chart under specified illumination. The disadvantage is that only a relatively small number of reflectance spectra can be included in the optimization, and an experimental set-up is needed for the illumination. However, an alternative statistical (computational) approach can be taken provided we have knowledge of the camera spectral responsivities, in which case any number of spectra can be included in the optimization, including models for an infinite set of spectra. The power of this approach is that desirable characteristics can be imposed on the set of spectra that could, for example, be related to assumed real-world conditions [20].

It is the above computational approach to camera characterization that provides the first application for the PF spectra introduced in this paper. Previous models for the autocorrelation matrix based upon an infinite set of spectra include Maximum Ignorance (MI) [20] and Maximum Ignorance with Positivity (MIP) [21,22]. MIP assumes that all random spectra normalized to the range [0,1] are equally likely, which means that the statistics cannot be varied and correlations between spectra are not included. The Minimal Knowledge I (MK-I) model for the autocorrelation matrix enables a measure of correlation to be included, albeit via an arbitrary Cauchy function [23], and Minimal Knowledge II (MK-II) enables the spectral statistics to be varied as a function of wavelength [24], but the underlying spectra themselves cannot be specified. Recently, a model for the autocorrelation matrix based upon piecewise-constant spectra was introduced [25]. However, the use of so-called normalized illumination [26] was required in order that the spectral statistics could be varied as a function of wavelength. On the other hand, the method introduced in the present paper is a much more flexible and useful approach since the piecewise-functional (PF) spectra directly generate the autocorrelation matrix.

Section 2 below begins by briefly summarizing the meaning of autocorrelation in the current context, and then provides a brief summary of the computational approach to camera characterization. The concept of PF spectra is then developed in Sec. 3, and an expression for the autocorrelation matrix is derived using a truncated normal probability distribution. Special cases are then discussed, including the case of piecewise-constant spectra. Section 4 demonstrates the flexibility of the model by tuning it to closely reproduce the autocorrelation matrices of several widely-used small real-world spectral reflectance datasets. In other words, it is shown that the autocorrelation matrices of such datasets can be represented by those of PF spectra. Although the PF autocorrelation matrices are generated by (trained upon) an infinite number of spectra, the color characterization performance is found to be almost as good as when using the dataset matrices themselves.

2. Background

Before developing the concept of PF spectra in Sec. 3, it is useful to review the meaning of autocorrelation in the current context, and to briefly summarize the computational approach to camera characterization.

Optics EXPRESS

2.1. Autocorrelation

Consider a $1 \times m$ row vector $\mathbf{s}$, where the elements s_i are spectral values (such as reflectance) sampled at a set of m wavelengths, $1 \le i \le m$. The sample autocorrelation matrix, $\mathbf{s}^\top \mathbf{s}$, contains the autocorrelations between all pairs of elements of the vector. Given a set of n such spectra, an $n \times m$ matrix S can be constructed, where each row contains a spectrum. In this case the elements of the sample autocorrelation matrix are defined by

$$\left[S^\top S\right]_{ij} = \frac{1}{n} \sum_{k=1}^{n} s_{ki}\, s_{kj}, \tag{1}$$

where normalization by the number of spectra, n, has been implicitly included. The sample autocorrelation matrix quantifies the similarity between values at different wavelength sample locations. Its matrix elements can alternatively be expressed in the form

$$\left[S^\top S\right]_{ij} = \sigma_{ij} + \mu_i \cdot \mu_j \tag{2a}$$

$$\sigma_{ij} = \rho_{ij} \cdot \sigma_i \cdot \sigma_j, \tag{2b}$$

where μ_i and μ_j are the means at sample locations i and j, while σ_{ij} is the autocovariance between the spectra at these locations. The latter can be expressed in terms of Pearson's correlation coefficients, ρ_{ij}, where σ_i and σ_j are the standard deviations [23]. Since $\rho_{ij} = 1$ when $i = j$, the diagonal matrix elements are $\sigma_i^2 + \mu_i^2$.

If the number of spectra $n \to \infty$, then the sample autocorrelation matrix becomes the true autocorrelation matrix of the underlying stochastic process, $S^\top S \to \Sigma_{SS}$. In Sec. 3, a method for finding Σ_{SS} in closed form is developed.

2.2. Camera characterization

Given the notation listed in the first ten lines of Table 1, let us assume that we have a set of n color-calibration reflectance spectra contained in an $n \times m$ matrix S, where each of the m columns represents a wavelength sample in the spectral passband. Given a characterization illuminant, which can be mathematically modeled by an $m \times m$ diagonal matrix E containing power per wavelength values, the color signal matrix can be defined as $C = SE$ [23,26]. Now consider the following,

$$A \propto CV^\top \tag{3a}$$

$$B \propto CR^\top. \tag{3b}$$

Here A is an $n \times 3$ matrix that models the human observer response, and so V is the $3 \times m$ matrix that contains the elements of the CIE color-matching functions, $x(\lambda)$, $y(\lambda)$, $z(\lambda)$. Each of the n rows of A are a triplet of XYZ values. Analogously, B is the $n \times 3$ matrix that models the camera responses to the same set of reflectance spectra under the illuminant E, and so R is a $3 \times m$ matrix that contains the camera spectral responsivities. Each of the n rows of B are a triplet of linear raw RGB values.

The goal is to find a 3×3 matrix M that best maps the n rows of linear RGB values to the n rows of XYZ values under the characterization illuminant, i.e. the matrix M that minimizes the error in the approximation $BM \approx A$. The least-squares solution is given by

$$M = (B^\top B)^{-1} B^\top A \tag{4a}$$

$$= \left(RE(S^\top S)ER^\top\right)^{-1} RE(S^\top S)EV^\top, \tag{4b}$$

where the second line follows by substituting Eqs. (3a) and (3b) into the first line and utilizing the fact that $C = SE$. The central object of interest is seen to be the spectral reflectance autocorrelation matrix, $S^\top S$.

Optics EXPRESS

Table 1. Table of notation

m	The number of sampled wavelengths in the spectral passband, e.g. $m = 301$ when sampling between 400-700 nm at 1 nm intervals.
n	The number of reflectance spectra in a dataset.
V	$3 \times m$ matrix containing the $x(\lambda)$, $y(\lambda)$, $z(\lambda)$ color-matching functions.
R	$3 \times m$ matrix containing the camera spectral responsivities. Each row is a color channel.
S	$n \times m$ matrix, where each row is a reflectance spectrum and each column is a particular wavelength sample.
E	$m \times m$ diagonal matrix containing the characterization illuminant.
C	$n \times m$ color-signal matrix defined by $C = SE$.
$S^\top S$	$m \times m$ sample reflectance autocorrelation matrix.
A	$n \times 3$ matrix where each row is a triplet of XYZ tristimulus values.
B	$n \times 3$ matrix where each row is a triplet of linear raw RGB values.
M	3×3 camera characterization matrix.
i, j	Sample locations in the spectral passband.
λ_i	Wavelength in the spectral passband at sample location i.
s_i	Spectral reflectance value at wavelength sample λ_i, i.e. $s_i \equiv s(\lambda_i)$.
a, b	Lower and upper limits for the s_i values.
$p(s_i)$	Probability density function for s_i.
μ_i	Mean for $p(s_i)$.
σ_i	Standard deviation for $p(s_i)$.
z_i	z-score for $p(s_i)$.
α	Correlation parameter, where $0 \leq \alpha < 1$.
$\langle L \rangle$	Expected length of the piecewise functions between jumps, as defined by Eq. (9).
Σ_{SS}	$m \times m$ reflectance autocorrelation matrix.
$\tilde{\mu}_i$	Mean for $p(s_i)$ before truncation, provided $p(s_i)$ is a truncated normal distribution.
$\tilde{\sigma}_i$	Standard deviation for $p(s_i)$ before truncation, provided $p(s_i)$ is a truncated normal distribution.
$\tilde{z}_i$	z-score for $p(s_i)$ before truncation, provided $p(s_i)$ is a truncated normal distribution.
$\phi(x)$	Exponential function defined by Eq. (12b).
Z_i	Normalization constant defined by Eq. (12d), which compensates for the truncation.

The absolute values of the entries in M will depend upon the values of the constants of proportionality that appear in Eqs. (3a) and (3b), however for practical applications M needs to be normalized. For example, a global scaling factor can be applied so that the maximum raw value in the green raw channel, G = 1, maps to Y = 1 for a white patch under the characterization illuminant [19].

3. Method

This section begins by introducing the concept of piecewise-functional (PF) spectra. In Sec. 3.2, PF spectra are used to construct an analytic model for the autocorrelation matrix, and subsequently a closed-form solution is obtained for the case of a truncated normal probability distribution. Finally, special cases are discussed in Sec. 3.3.

3.1. Piecewise-functional spectra

Let m be the number of wavelength samples in the model spectra. For example, if the spectral passband is taken to be between 400-700 nm and sampled at 1nm intervals then $m = 301$, in

Optics EXPRESS

which case

$$\lambda_i = 399 + i, \quad i = 1, 2 \cdots 301. \tag{5}$$

Again, let $s_i \equiv s(\lambda_i)$ denote the spectral value at wavelength sample i. These values could be normalized, for example $s \in [a, b] = [0, 1]$. For model spectra with statistics that vary as a function of wavelength, the probability density function, $p(s_i)$, will be sample-location dependent.

Let s_i at sample location i take a random value in the range $[a, b]$ according to a specified $p(s_i)$. Now let us build in correlation between sample locations by assigning a probability α that the adjacent sample s_{i+1} (where λ_{i+1} is the subsequent wavelength) takes the same *relative* value as $s(\lambda_i)$. Specifically, let s_{i+1} take a value that is the same number of standard deviations away from the means at these two sample locations. This can be defined by the z-score at sample location i,

$$z_i = \frac{s_i - \mu_i}{\sigma_i}, \tag{6}$$

where μ_i and σ_i are the mean and standard deviation corresponding to $p(s_i)$. In other words, let us assign α to be the probability that the adjacent sample takes a value that has the same z-score,

$$s_{i+1} = z_i . \sigma_{i+1} + \mu_{i+1}, \tag{7}$$

where μ_{i+1} and σ_{i+1} are the mean and standard deviation for $p(s_{i+1})$. Mathematically,

$$P\left(z_{i+1} = z_i\right) = \alpha \tag{8a}$$

$$P\left(z_{i+1} \neq z_i\right) = 1 - \alpha, \tag{8b}$$

where $0 \leq \alpha \leq 1$. If $z_{i+1} \neq z_i$, then the value s_{i+1} is instead drawn according to $p(s_{i+1})$. Repeating the above process at all wavelength samples in the range specified by Eq. (5) defines an algorithm that can be implemented numerically in order to randomly generate as many spectra as desired.

Clearly, the sections of a randomly generated spectrum where $z_{i+1} = z_i$ will have a functional form that depends upon the underlying statistics, specifically how the mean and standard deviation vary as a function of wavelength. On the other hand, whenever $z_{i+1} \neq z_i$, a "jump" will be encountered since the value s_{i+1} will be drawn at random according to $p(s_{i+1})$. In other words, piecewise sections between jumps contain correlated values since they have the same z-score. On the other hand, values that belong to different piecewise sections are uncorrelated. The degree of correlation between values at different sample locations will depend upon α. A larger α will increase the average or expected length of the piecewise-functional sections between jumps, $\langle L \rangle$. In fact, it is shown in Appendix A that

$$\langle L \rangle = (1 - \alpha)^{-1} . \tag{9}$$

For example, in Fig. 1 a fixed standard deviation is kept but a simple linear increase in the mean, $\mu_i \equiv \mu(\lambda_i)$, is defined when moving along the spectral passband. In this case the sections between jumps are piecewise linear. Figures 1(a) and (b) show examples of randomly generated spectra for two different α values, specifically $\alpha = 0.5$, which corresponds to $\langle L \rangle = 2$ nm, and $\alpha = 0.98$, which corresponds to $\langle L \rangle = 50$ nm.

3.2. Model autocorrelation matrix

In order to derive a closed-form expression for the autocorrelation matrix elements, consider the construction described above in the context of two general sample locations i and j. The probability that the z-score z_k will be the same as z_i for all $i < k \leq j$, i.e. there will be a

Optics EXPRESS

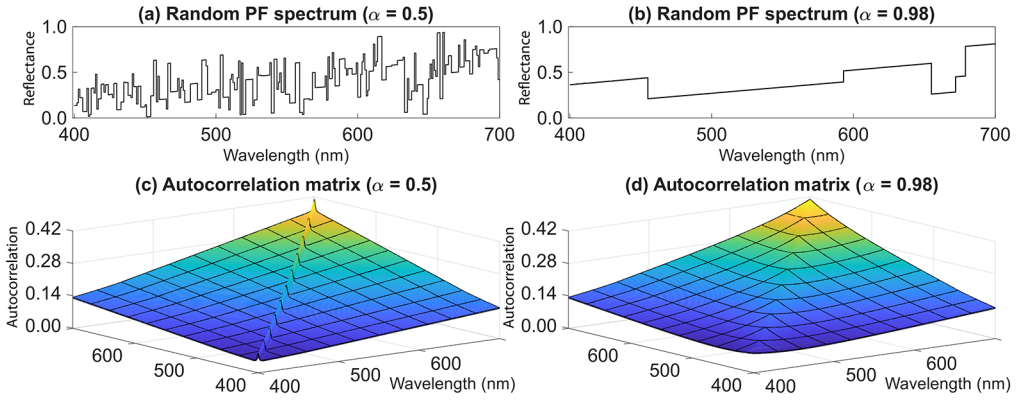

Fig. 1. (a) Randomly generated PF spectrum with a linear-ramp mean from $\mu = 0.2$ ($\lambda =$ 400 nm) to $\mu = 0.6$ ($\lambda = 700$ nm), fixed standard deviation $\sigma = 0.22$, and $\alpha = 0.5$. (b) Same as (a) but with $\alpha = 0.98$. (c) Autocorrelation matrix for the infinite set of PF spectra with statistics corresponding to (a). (d) Autocorrelation matrix for the infinite set of PF spectra with statistics corresponding to (b).

piecewise-functional section of length $|j - i|$ samples, and the probability that the z-score will be different, are respectively given by

$$P\left(z_k = z_i,\ i<k \le j\right) = \alpha^{|j-i|} \tag{10a}$$

$$P\left(z_j \neq z_i\right) = 1 - \alpha^{|j-i|}. \tag{10b}$$

By utilizing Eqs. (7) and (10), the matrix elements of the autocorrelation matrix can now be analytically expressed as follows,

$$\begin{aligned}[\Sigma_{SS}]_{ij} = \ & \alpha^{|j-i|} \int_a^b p(s_i)\, s_i\left(z_i.\, \sigma_j + \mu_j\right) ds \\ & + \left(1 - \alpha^{|j-i|}\right) \int_a^b p(s_i) s_i\, ds \int_a^b p(s_j) s_j\, ds.\end{aligned} \tag{11}$$

Significantly, it is possible to integrate over an infinite set of model PF spectra and obtain a closed-form solution. If PF spectra are generated numerically according to the construction described in Sec. 3.1, then the sample autocorrelation matrix calculated numerically will converge towards this closed-form solution as the number of generated spectra increases.

3.2.1. Truncated normal probability distribution

The parameter α describes how correlated the values of neighboring spectral samples are with each other. On the other hand, the probability density function $p(s)$ describes how likely the sample value in question will occur in the first place.

In order to have complete control over μ and σ, let us consider a normal distribution, which can be varied at each wavelength sample location. However, the distribution must be truncated according to $[a, b]$ at all wavelengths since $[a, b]$ defines the range of allowed spectral values [27]. In other words, $p(s_i)$ must be defined by the truncated normal distribution (e.g. Reference [28]),

$$p(s_i) = \frac{1}{\tilde{\sigma}_i Z_i}\, \phi(\tilde{z}_i(s_i)) \tag{12a}$$

$$\phi(x) = \frac{1}{\sqrt{2\pi}} \exp\left(-\frac{1}{2}x^2\right) \tag{12b}$$

Optics EXPRESS

$$\tilde{z}_i(s_i) = \frac{s_i - \tilde{\mu}_i}{\tilde{\sigma}_i} \tag{12c}$$

$$Z_i = \frac{1}{2}\left(\mathrm{erf}\left(\frac{\tilde{z}_i(b)}{\sqrt{2}}\right) - \mathrm{erf}\left(\frac{\tilde{z}_i(a)}{\sqrt{2}}\right)\right), \tag{12d}$$

where $\tilde{z}_i$ defines the z-score at sample location i, and the normalization constant Z_i compensates for the truncation. The error function, erf, is a standard integral [29].

As illustrated by example in Fig 2, the truncation will in general alter the mean and standard deviation of the untruncated distribution. In this paper, the tilde symbol denotes untruncated values, so $\tilde{\mu}$ and $\tilde{\sigma}$ are the mean and standard deviation before the truncation, which become μ and σ afterwards. The latter are our target values, such as those corresponding to some statistical model or even a real-world dataset. Consequently, at each sample location, it will in general be necessary to find values for the input mean and standard deviation, $\tilde{\mu}$ and $\tilde{\sigma}$, that will become our target values after the truncation, μ and σ. This problem can be easily solved by referring to Appendix B.

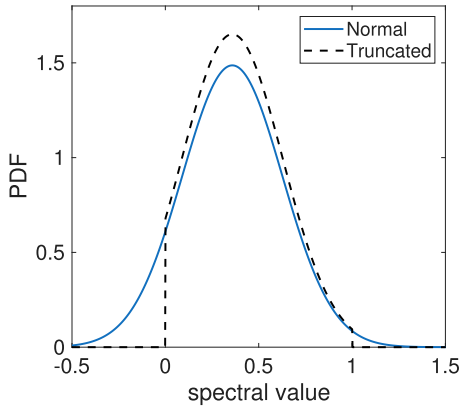

Fig. 2. The dashed black curve shows the probability density function for a truncated normal distribution in the range $[a, b] = [0, 1]$ with mean $\mu = 0.4$ and standard deviation $\sigma = 0.22$. According to Appendix B, the required input normal distribution illustrated by the solid blue curve must have a mean $\tilde{\mu} = 0.3521$ and standard deviation $\tilde{\sigma} = 0.2866$.

Inserting Eq. (12) into (11) and analytically performing the integration leads to the following closed-form solution for the autocorrelation matrix,

$$[\Sigma_{SS}]_{ij} = c_{1,i}\,\alpha^{|j-i|} + c_{2,i}\,c_{2,j}\left(1 - \alpha^{|j-i|}\right), \tag{13}$$

where the constants $c_{1,i}$, $c_{2,i}$ and $c_{2,j}$ are defined by

$$c_{1,i} = \frac{\tilde{\sigma}_j}{\tilde{\sigma}_i}\left(\sigma_i^2 + \mu_i^2 + \mu_i\left(\tilde{\mu}_j\frac{\tilde{\sigma}_i}{\tilde{\sigma}_j} - \tilde{\mu}_i\right)\right) - \tag{14a}$$

$$\frac{\sigma_i}{Z_i}\left\{\left(\frac{\tilde{\sigma}_j}{\tilde{\sigma}_i}(b + \mu_i - \tilde{\mu}_i) + \tilde{\mu}_j\right)\phi(z_i(b)) - \left(\frac{\tilde{\sigma}_j}{\tilde{\sigma}_i}(a + \mu_i - \tilde{\mu}_i) + \tilde{\mu}_j\right)\phi(z_i(a))\right\} \tag{14b}$$

$$c_{2,i} = \mu_i - \frac{\sigma_i}{Z_i}\{\phi(z_i(b)) - \phi(z_i(a))\}$$

Optics EXPRESS

$$c_{2,j} = \mu_j - \frac{\sigma_j}{Z_j}\left\{\phi(z_j(b)) - \phi(z_j(a))\right\}. \tag{14c}$$

Note that $z(a)$ and $z(b)$ are the z-scores corresponding to the minimum and maximum allowed spectral values after the truncation, i.e. $z(a) = (a-\mu)/\sigma$ and $z(b) = (b-\mu)/\sigma$, whereas Z depends upon $\tilde{z}(a)$ and $\tilde{z}(b)$.

Although the above equations may appear complicated at first glance, it should be emphasized that c_1, $c_{2,i}$ and $c_{2,j}$ are simply constants. The only input information required is the target mean and standard deviation of the truncated normal distribution, μ_i and σ_i, at each sample location i, where the truncation is to the range $[a, b]$. As mentioned above, the input means and standard deviations before the truncation, $\tilde{\mu}_i$ and $\tilde{\sigma}_i$, can be found according to Appendix B.

Figures 1(c) and (d) show the autocorrelation matrices calculated using Eq. (13) that correspond to the infinite set of spectra that have the same statistics as the example random spectra shown in Figs. 1(a) and (b), respectively. The mean and standard deviation of the spectra are the same in both cases but (a) and (c) correspond to $\alpha = 0.5$, which is equivalent to an expected step length $\langle L\rangle = 2$ nm, whereas (b) and (d) correspond to $\alpha = 0.98$, which is equivalent to $\langle L\rangle = 50$ nm. Evidently, the height and offset of the autocorrelation matrices are seen to be the same in both cases as this depends only upon μ and σ. On the other hand, increasing correlation between samples by increasing α leads to a wider autocorrelation matrix where the central peak that is present along the main matrix diagonal widens [11,30].

3.3. Special cases

An interesting special case is when the spectral statistics do not vary as a function of wavelength, i.e. $\mu_i = \mu$ and $\sigma_i = \sigma$ for all i. According to Eqs. (6) and (7), in this case $z_{i+1} = z_i$ simply means that $s_{i+1} = s_i$. In other words, the piecewise-functional (PF) spectra become perfectly piecewise constant [25] as shown in Fig. 3(a) and (b) for two different α values, specifically $\alpha = 0.8$ and 0.98. Equations (13) and (14) reduce to

$$[\Sigma_{SS}]_{ij} = c_1\,\alpha^{|j-i|} + c_2^2\left(1 - \alpha^{|j-i|}\right), \tag{15}$$

where the constants c_1 and c_2 are defined by

$$c_1 = \sigma^2 + \mu^2 - \frac{\sigma}{Z}\{(b+\mu)\,\phi(z(b)) - (a+\mu)\,\phi(z(a))\} \tag{16a}$$

$$c_2 = \mu - \frac{\sigma}{Z}\{\phi(z(b)) - \phi(z(a))\}. \tag{16b}$$

Since the autocorrelation statistics are now shift invariant, the autocorrelation matrix takes a so-called Toeplitz form [31,32] where all elements along a given matrix diagonal have the same value. In the present context, the autocorrelation matrix is a symmetric Toeplitz matrix where corresponding diagonals each side of the main diagonal are identical. The widening of the autocorrelation matrix when increasing α that was mentioned earlier is clearly evident in Figs. 3(c) and (d).

A similar special case where the statistics do not vary as a function of wavelength is that of a uniform probability distribution, $p(s) = 1/(b-a)$, which leads to the following closed-form result previously obtained in Ref. [25],

$$[\Sigma_{SS}]_{ij} = \frac{a^2 + ab + b^2}{3}\,\alpha^{|j-i|} + \frac{(a+b)^2}{4}\left(1 - \alpha^{|j-i|}\right). \tag{17}$$

In this case Σ_{SS} is again a Toeplitz matrix and the model spectra are again piecewise constant, but the mean and standard deviation are fixed according to the range $s \in [a, b]$ with values $\mu = (a+b)/2$ and $\sigma = 1/\sqrt{12}$, respectively, and so Eq. (17) is much less useful than Eq. (15). Indeed,

Optics EXPRESS

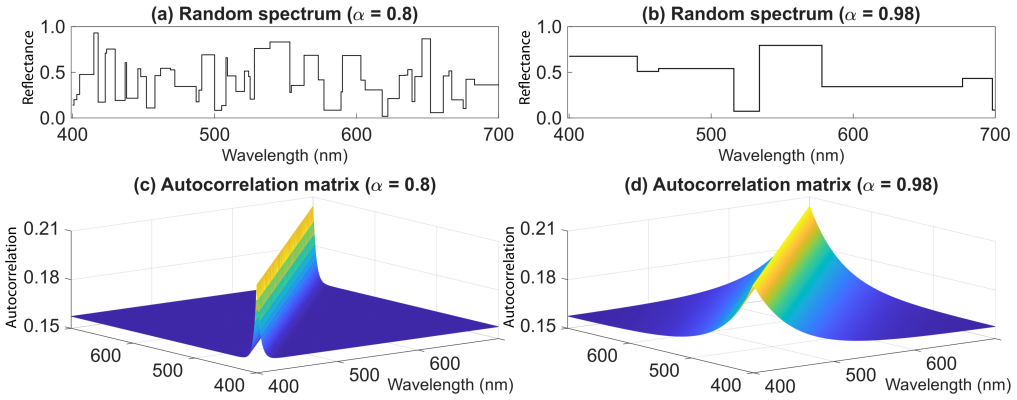

Fig. 3. (a) Randomly generated piecewise-constant spectrum with $\mu = 0.4$, $\sigma = 0.22$, and $\alpha = 0.8$. (b) Same as (a) but with $\alpha = 0.98$. (c) Autocorrelation matrix for the infinite set of piecewise-constant spectra with statistics corresponding to (a). (d) Autocorrelation matrix for the infinite set of piecewise-constant spectra with statistics corresponding to (b).

in Ref. [25] it was necessary to apply scale and offset parameters to Σ_{SS} in order to simulate altering μ and σ. Additionally, a wavelength dependence in the spectral statistics was simulated by the use of so-called normalized illumination [25,26], which is not needed when using the method developed in the present paper.

A more general case is where the correlation parameter α is allowed to vary as a function of wavelength. In Eq. (10), α is raised to the power $|j - i|$, which indicates that the correlation is shift invariant since wavelength dependence has not been included. However, if desired, α can be varied as a function of wavelength according to any specified model, in which case $\alpha \rightarrow \alpha(\lambda_i) \equiv \alpha_i$. In order to generalize the equations, it is necessary to take the product of all α_k values between sample locations i and j, which simply means making the following replacement,

$$\alpha^{|j-i|} \rightarrow \prod_{i=k}^{j} \alpha_k, \tag{18}$$

where k will either increase or decrease from i to j, depending on whether i is smaller or larger than j, respectively. The associated model spectra will again be piecewise functional (PF), however the expected length of the PF sections between jumps, $\langle L \rangle$, can vary along the spectral passband.

4. Results

In order to demonstrate the utility and flexibility of the approach, here we use piecewise functional (PF) spectra to try to closely replicate the autocorrelation matrices of several small real-world reflectance datasets. The first is the widely used 170 objects dataset (170-OBJ), which contains measured reflectances for various natural and man-made objects [1]. The second is the 462 Munsell dataset of color chips (462-MUN) [33], and the third is the 289 Agfa ColorReference dataset (289-AGF) that is used for calibrating color scanners [3]. All datasets were restricted to the 400-700 nm range and interpolated to 1 nm increments.

Let us first consider the 170-OBJ dataset. Figure 4(a) shows the mean $\mu(\lambda)$ and standard deviation $\sigma(\lambda)$ of these spectra as a function of wavelength. The mean is seen to monotonically increase, which leads to higher autocorrelation at longer wavelengths, as illustrated in Fig. 4(c). Indeed, this is a trend that is generally observed for real-world measured reflectance datasets. We substituted $\mu(\lambda)$ and $\sigma(\lambda)$ into Eq. (13), which is the closed-form expression for the autocorrelation

Optics EXPRESS

matrix obtained using PF spectra. (The input $\tilde{\mu}(\lambda)$ and $\tilde{\sigma}(\lambda)$ required before truncating the normal distribution were found at each wavelength sample location according to Appendix B). The optimum α value that minimizes the difference between the dataset and PF spectra autocorrelation matrices was then found by minimizing the following percentage error metric [6],

$$\%\ \text{error} = 100 \cdot \frac{\left\|\Sigma_{SS} - S^{\top}S\right\|^2}{\left\|S^{\top}S\right\|^2}, \tag{19}$$

where Σ_{SS} is the PF spectra autocorrelation matrix, $S^{\top}S$ is the 170-OBJ autocorrelation matrix, and $\|\cdot\|$ denotes the Frobenius norm. The α value was found to be $\alpha = 0.9974$, which corresponds to an expected piecewise-function length $\langle L\rangle = 385$ nm. This indicates strong correlation between the spectra, which is evident if the original 170 spectra themselves are plotted. The PF spectra autocorrelation matrix is shown in Fig. 4(d). The maximum difference between the autocorrelation matrices of Figs. 4(c) and (d) is found to be just 1.77% according to Eq. (19), which indicates very strong similarity. This is a significant result given the fact that the PF autocorrelation matrix has been generated using an infinite number of spectra.

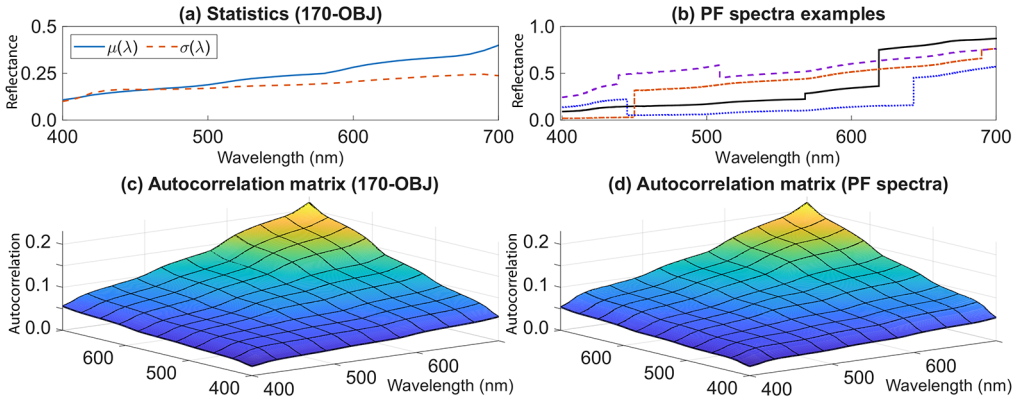

Fig. 4. (a) Spectral statistics (mean μ and standard deviation σ) of the 170-OBJ dataset [1] resampled at 1 nm increments in the range $[a, b] = [0.0067, 0.9123]$. (b) Examples of randomly generated PF spectra with the same μ and σ as 170-OBJ and $\alpha = 0.9974$. (c) Autocorrelation matrix corresponding to 170-OBJ. (d) Autocorrelation matrix corresponding to the infinite set of PF spectra described in (b).

Interestingly, the above result was obtained without the need to let the correlation parameter α be wavelength dependent. In other words, the correlation between the spectra in 170-OBJ is essentially independent of wavelength, and this finding appears to hold true in general for measured reflectance datasets. Figure 4(b) shows examples of random PF spectra numerically generated according to the construction described in Sec. 3.1. Unlike Figs. 1(a) and (b), which correspond to a linear-ramp mean, here $\mu(\lambda)$ and $\sigma(\lambda)$ correspond to the mean and standard deviation of a real-world dataset, and so the PF sections in-between jumps are seen to vary in a nonlinear manner that depends upon the statistics of the target dataset. Note that $\mu(\lambda)$ and $\sigma(\lambda)$ could also be parameterized using a simple model if desired.

In order to see how closely the piecewise-functional (PF) spectra can replicate the camera characterization performance achieved using 170-OBJ, Eq. (4b) was used to characterize a camera. The spectral responsivities for the Nikon D700 camera measured by Jiang *et al.* [34] were selected, along with CIE illuminants A and D65 as representative illuminations. Firstly, a characterization matrix M was calculated according to Eq. (4b) using the reflectance autocorrelation matrix for 170-OBJ, which yields a set of 170 approximate triplets of XYZ values contained in the 170×3

Optics EXPRESS

matrix A according to $BM \approx A$, where B is the 170×3 matrix that contains triplets of camera raw values. These colors were compared with the reference XYZ values defined by Eq. (3a) and the mean and 95$^{\text{th}}$ percentile color errors were calculated in terms of ΔE^* using the CIE 1976 color difference formula. These least-squares (LS) results, one for each illuminant, are shown in the first data column of Table 2. These are our target values since the training and testing datasets are the same, and hence the % error will be zero according to Eq. (19).

Table 2. Results for 170-OBJ

	LS	PF	MIP	MK-II
Correlation		$\alpha = 0.9974$	$\alpha' = 0$	$\alpha' = 221$
Error %	0.00	**1.77**	139.44	2.11
Mean ΔE^* (A)	2.09	**2.39**	3.68	4.11
p95 ΔE^* (A)	5.89	**6.86**	9.99	14.47
Mean ΔE^* (D65)	1.86	**2.25**	2.98	3.44
p95 ΔE^* (D65)	5.76	**7.58**	7.83	14.07

The second data column of Table 2 lists the results obtained when $BM \approx A$ is instead solved using the PF autocorrelation matrix that is closest in terms of % error to the 170-OBJ autocorrelation matrix, as described above, and then the characterization performance tested using the 170-OBJ spectra. Significantly, the mean and 95$^{\text{th}}$ percentile ΔE^* are seen to be close to the target LS results. For comparison purposes, other state-of-the art methods based upon an infinite number of spectra were implemented, namely MIP and MK.

Firstly, recall that MIP assumes an infinite number of completely uncorrelated spectra, which is equivalent to the use of Eq. (17) with $\alpha = 0$, which leads to a Toeplitz autocorrelation matrix with a very narrow peak (see Refs. [21,25] and Fig. 3(c) for reference). Consequently, the % error for the MIP autocorrelation is found to be very large, as evident from the third data column in Table 2, and this leads to higher ΔE^* results. Note that in principle, there is no upper bound on the % error calculated using Eq. (19). Secondly, MK-I models the autocorrelation matrix via Eqs. (2a) and (2b) with correlation defined arbitrarily by

$$\rho_{ij} = \frac{\alpha'^2}{\alpha'^2 + (\lambda_i - \lambda_j)}, \tag{20}$$

where α' is the width in nm at which ρ_{ij} falls to 1/2, and so α' here does not have the same meaning as the α parameter for PF spectra defined by Eq. (8a). MK-I assumes a uniform probability distribution, which leads to Toeplitz autocorrelation matrices that resemble Fig. 3(d). In this case, it turns out that $\alpha' = 0$ actually minimizes Eq. (19), and so MK-I is not able to improve upon MIP in terms of % error. Therefore only MK-II was implemented here, where it is possible to use the $\mu(\lambda)$ and $\sigma(\lambda)$ that correspond to the 170-OBJ dataset itself in Eqs. (2a) and (2b) and determine the α value that minimizes the % error. As seen in the fourth data column of Table 2, the closest matching autocorrelation matrix was found to have 2.11% error, which is small, however the ΔE^* results are actually worse than MIP. This reveals the sensitivity of the ΔE^* calculation when attempting to reproduce a highly structured autocorrelation matrix using the arbitrary MK-II correlation defined by Eq. (20).

It should be pointed out that it is possible to use MK-I (and MK-II) to find autocorrelation matrices that yield lower ΔE^* than MIP for datasets such as 170-OBJ, even though the % error of the autocorrelation matrices may be higher. This possibility can occur because the characterization is performed in the linear domain using Eq. (4b) whereas ΔE^* is evaluated in a nonlinear domain. However, the aim in the present context is to try to minimize the % error in the autocorrelation matrix and then evaluate the resulting color error.

Optics EXPRESS

The above experiment was repeated using the 462-MUN and 289-AGF datasets. The autocorrelation matrices are shown in Fig. 5(a) and (c), respectively, and the results are given in Tables 3 and 4, respectively. In both cases, small % errors were found for the PF autocorrelation matrices shown in Fig. 5(b) and (d) respectively, which again indicates that the correlation is independent of wavelength. Again, the results for ΔE^* are close to the LS results. The MK-II results are seen to be close to MIP for both 462-MUN and 289-AGF, and ΔE^* is improved compared to MIP for illuminant A.

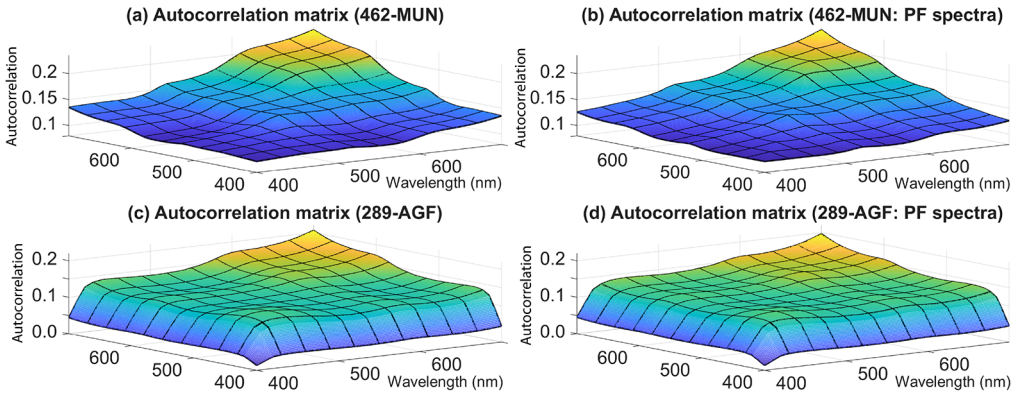

Fig. 5. (a) Autocorrelation matrix for the 462-MUS dataset. (b) PF spectra autocorrelation matrix for the 462-MUS dataset. (c) Autocorrelation matrix for the 289-AGF dataset. (b) PF spectra autocorrelation matrix for the 289-AGF dataset.

Table 3. Results for 462-MUN

	LS	PF	MIP	MK-II
Correlation		$\alpha = 0.9973$	$\alpha' = 0$	$\alpha' = 205$
Error %	0.00	**2.51**	63.53	3.09
Mean ΔE^* (A)	1.71	**1.82**	3.09	2.59
p95 ΔE^* (A)	5.29	**5.07**	8.16	8.83
Mean ΔE^* (D65)	1.57	**1.79**	2.44	2.55
p95 ΔE^* (D65)	5.14	**5.95**	6.25	8.54

Table 4. Results for 289-AGF

	LS	PF	MIP	MK-II
Correlation		$\alpha = 0.9979$	$\alpha' = 0$	$\alpha' = 229$
Error %	0.00	3.20	92.05	**2.65**
Mean ΔE^* (A)	0.92	**0.94**	2.09	1.65
p95 ΔE^* (A)	2.97	**2.98**	5.56	4.89
Mean ΔE^* (D65)	0.82	**1.05**	1.70	1.70
p95 ΔE^* (D65)	2.51	**3.73**	4.54	5.87

5. Discussion

In the previous section, the optimal matrix transformations (in a least-squares sense) from the camera raw space to CIE XYZ were calculated for several small real-world datasets, namely

Optics EXPRESS

170-OBJ, 462-MUN and 289-AGF. However, as mentioned in the introduction, cameras will in reality record output pixel values that originate from a mixture of such spectra, and the question as to what is the optimal set of spectral reflectances for camera characterization is an interesting question. Indeed, the ranking of algorithms may change depending on the datasets used [6]. Certainly, camera manufacturers may use their own proprietary sets of reflectance spectra.

Recently, it was proposed that the space of reflectance spectra should be integrated over rather than sampled [6]. However, a drawback of the computational approach introduced in Ref. [6] is that unphysical spectra are included, in other words spectra that could not be encountered in the real world. Indeed, negative percentage reflectance is admitted in the model [6].

In this paper, a model for piecewise functional (PF) spectra has been presented, and it has been shown that an infinite number of such spectra that satisfy a given probability density function can be analytically integrated over (and also numerically generated up to a given finite number). For the analytic integration, a solution for the autocorrelation matrix was found in closed form. The important point here is that the resulting matrix transformation has been optimized (again in a least-squares sense) for an infinite number of spectra that satisfy the specified statistics (mean and standard deviation) according to the specified probability density function, and therefore will be expected to perform better for unseen data. For example, in Fig. 4(b), spectra that are similar in appearance to those of 170-OBJ were presented. However, our optimization also includes spectra that could be very different. For example, Fig. 6(b) shows several other example PF spectra tuned to the same statistics as 170-OBJ. (The 170-OBJ spectral reflectance curves themselves are plotted in Fig. 6(a)). Indeed, it is remarkable that the matrix optimized for an infinite number of PF spectra can, when tuned to the same statistics as 170-OBJ, approach the performance of the matrix optimized for the small 170-OBJ dataset itself when tested on 170-OBJ.

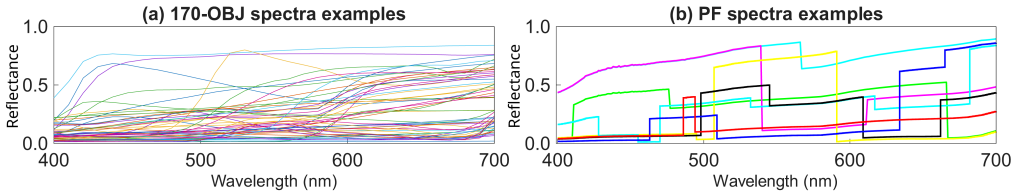

Fig. 6. (a) Spectral reflectance curves for the 170-OBJ dataset [1] resampled at 1 nm increments in the range $[a, b] = [0.0067, 0.9123]$. For clarity, only every third curve is plotted, i.e. a total of 56 curves. (b) More examples of randomly generated PF spectra with the same μ and σ as 170-OBJ and $\alpha = 0.9974$.

The construction presented in this paper therefore presents a very useful investigative tool, not only in the context of camera characterization, but also as a means of generating all possible spectra that satisfy given statistics. In the context of camera color characterization, an immediate application would be to find the parameters that give the lowest overall cross-validated color error when tested on a large collection of real-world measured datasets.

6. Conclusion

This paper has introduced the concept of piecewise-functional (PF) spectra as a tool for modeling autocorrelation statistics in the context of reflectance and color-signal spectra. Significantly, PF spectra can be generated numerically, and an infinite number of such spectra can be analytically integrated over to directly obtain the autocorrelation matrix in closed form.

The first application has centered upon the statistical (computational) method for camera characterization, where PF reflectance spectra were used to generate autocorrelation matrices that closely matched those of widely used small real-world measured reflectance datasets. Indeed, even though the PF autocorrelation matrices were trained upon an infinite number of spectra, the

Optics EXPRESS

characterization performance was found to be almost as good as when using the autocorrelation matrices optimized for the real-world datasets themselves when tested on those datasets. Due to the simplicity and flexibility of the model, we anticipate its application both as a closed-form representation of autocorrelation and as an investigative tool.

Appendix A

It is possible to derive an expression for the expected length (denoted here as $\langle L \rangle$) of the piecewise-functional sections in-between jumps in terms of α [30]. To proceed, consider a randomly generated spectral value, $s_i \equiv s(\lambda(i))$ at wavelength sample λ_i. The probability that the adjacent value s_{i+1} does *not* have the same z-score is $1-\alpha$, in which case $\langle L \rangle = 1$. The probability that s_i is only extended to a piecewise section by one wavelength sample (so that only s_{i+1} has the same z-score) is $\alpha(1-\alpha)$, in which case $\langle L \rangle = 2$. Continuing this argument, if s_j is located n wavelength samples away from i, the probability that s_i is extended to a piecewise-functional section (where all values have the same z-score) with total length $\langle L \rangle = k$ is $\alpha^{k-1}(1-\alpha)$ if $k<n$ and α^{k-1} if $k = n$. Therefore

$$\langle L \rangle = \left((1-\alpha) \sum_{k=1}^{n-1} k\alpha^{k-1} \right) + n\alpha^{n-1} = \frac{1-\alpha^n}{1-\alpha}. \tag{21}$$

Finite piecewise-functional sections are obtained provided that $0 \leq \alpha < 1$, in which case taking the limit $n \to \infty$ yields Eq. (9).

Appendix B

Consider the truncated normal distribution defined by Eq. (12) that has been truncated to the range $[a, b]$. The mean and standard deviation after the truncation, μ and σ, are defined by

$$\mu = \tilde{\mu} - \frac{\tilde{\sigma}}{Z}(\phi(\tilde{z}(b)) - \phi(\tilde{z}(a))) \tag{22a}$$

$$\sigma = \tilde{\sigma}\sqrt{1 - \frac{\tilde{z}(b)\phi(\tilde{z}(b)) - \tilde{z}(a)\phi(\tilde{z}(a))}{Z} - \left(\frac{\phi(\tilde{z}(b)) - \phi(\tilde{z}(a))}{Z}\right)^2}, \tag{22b}$$

where $\tilde{\mu}$ and $\tilde{\sigma}$ are the values before the truncation. Here ϕ and Z have been defined by Eqs. (12b) and (12d), and $\tilde{z}(a)$ and $\tilde{z}(b)$ are the z-scores of a and b (the minimum and maximum spectral values) before the truncation, $\tilde{z}(a) = (a-\tilde{\mu})/\tilde{\sigma}$ and $\tilde{z}(b) = (b-\tilde{\mu})/\tilde{\sigma}$. In order to generate spectra with the target μ and σ, the required input $\tilde{\mu}$ and $\tilde{\sigma}$ can be straightforwardly found by moving the RHS of Eqs. (22a) and (22b) to the LHS, inserting the target μ and σ, and finding the roots of the equations. An initial guess is provided by μ and σ.

Funding. Engineering and Physical Sciences Research Council (EP/S028730/1).

Acknowledgement. D A Rowlands acknowledges support from the University of East Anglia, UK.

Disclosures. The authors declare no conflicts of interest.

Data availability. Datasets underlying the results presented in this paper are available in Refs. [1,3,33,34]. Data presented in this paper are not publicly available at this time but may be obtained from the authors upon reasonable request.

References

1. M. J. Vrhel, R. Gershon, and L. S. Iwan, "Measurement and analysis of object reflectance spectra," Color Res. Appl. **19**(1), 4–9 (1994).
2. J. P. S. Parkkinen, J. Hallikainen, and T. Jaaskelainen, "Characteristic spectra of Munsell colors," J. Opt. Soc. Am. A **6**(2), 318–322 (1989).

Optics EXPRESS

3. Computational Spectral Imaging Research Group, University of Eastern Finland, https://sites.uef.fi/spectral/databases-software.
4. K. Barnard, L. Martin, B. Funt, *et al.*, "A data set for colour research," Color Res. Appl. **27**(3), 147–151 (2002).
5. A. Gutiérrez, B. Silva, J. M. Fanchini, *et al.*, "Spectral dataset of natural objects? reflectance from the Southern cone of South America," Sci. Data **12**(1), 594 (2025).
6. G. D. Finlayson, J. Vazquez-Corral, and F. Fang, "Integrating the space of reflectance spectra," IEEE Trans. on Image Process. **34**, 2588–2601 (2025).
7. D. A. Forsyth, "A novel algorithm for color constancy," International Journal of Computer Vision **5**(1), 5–35 (1990).
8. E. Schrödinger, "Theory of pigments of greatest lightness," Ann. Phys. **367**, 603–622 (1920).
9. A. D. Logvinenko, "An object-color space," Journal of Vision **9**(11), 5 (2009).
10. A. C. Hurlbert and T. A. Poggio, "Synthesizing a color algorithm from examples," Science **239**(4839), 482–485 (1988).
11. D. A. Rowlands and G. D. Finlayson, "Optimisation of convolution-based image lightness processing," J. Imaging **10**(8), 204 (2024).
12. International Organization for Standardization, "Graphic technology and photography ? Colour characterisation of digital still cameras (DSCs) ? Part 1: Stimuli, metrology and test procedures," ISO 17321-1 (2012).
13. P. C. Hung, "Sensitivity metamerism index for digital still camera," in *Proc. SPIE; Color Science and Imaging Technologies*, vol. 4922 (2002), pp. 1–14.
14. Y. Li, Y. Li, N. Liao, *et al.*, "Colorimetric characterization of the wide-color-gamut camera using the multilayer artificial neural network," J. Opt. Soc. Am. A **40**(3), 629–636 (2023).
15. Y. Li, N. Liao, Y. Li, *et al.*, "Color conversion of wide-color-gamut cameras using optimal training groups," Sensors **23**(16), 7186 (2023).
16. X. Jia, Y. Li, H. Gu, *et al.*, "Improved multi-input parameter optimization method for camera colorimetric characterization," J. Opt. Soc. Am. A **41**(8), 1601–1610 (2024).
17. A. Kucuk, G. D. Finlayson, R. Mantiuk, *et al.*, "Performance comparison of classical methods and neural networks for colour correction," J. Imaging **9**(10), 214 (2023).
18. K. E. Spaulding, R. M. Vogel, and J. R. Szczepanski, "Method and apparatus for color correcting multi-channel signals of a digital camera," U.S. Patent 5805213A, 1998.
19. D. A. Rowlands, "Color conversion matrices in digital cameras: a tutorial," Opt. Eng. **59**(11), 110801 (2020).
20. P. L. Vora and H. J. Trussell, "Measure of goodness of a set of color-scanning filters," J. Opt. Soc. Am. A **10**(7), 1499–1508 (1993).
21. G. D. Finlayson and M. S. Drew, "The Maximum Ignorance Assumption with Positivity," in *Proc. IS&T/SID Fourth Color Imaging Conference: Color Science, Systems and Applications*, (1996), pp. 202–205.
22. G. D. Finlayson, J. Vazquez-Corral, and F. Fang, "The Discrete Cosine Maximum Ignorance Assumption," in *Proc. IS&T 29th Color and Imaging Conference*, (2021), pp. 14–18.
23. J. A. S. Viggiano, "Minimal-Knowledge Assumptions in Digital Still Camera Characterization I: Uniform Distribution, Toeplitz Correlation," in *Proc. IS&T/SID 9th Color Imaging Conference: Color Science and Engineering: Systems, Technologies, Applications*, (2001), pp. 332–336.
24. J. A. S. Viggiano, "Minimal-Knowledge Assumptions in Digital Still Camera Characterization II: Non-Uniform Distribution," in *Proc. IS&T PICS Conference*, (2003), pp. 435–440.
25. D. A. Rowlands and G. D. Finlayson, "Piecewise-constant reflectance spectra, their autocorrelation, and their application in camera characterisation," in *Proceedings of the 12th Colour and Visual Computing Symposium (CVCS 2024), Gjovik, Norway, September 5-6, 2024.*, (2024).
26. G. D. Finlayson and J. Paul, "Minimal Knowledge versus the Real World," in *Proc. IS&T/SID Tenth Color Imaging Conference: Color Science, Systems and Applications*, (2002), pp. 133–138.
27. D. H. Brainard and W. T. Freeman, "Bayesian color constancy," J. Opt. Soc. Am. A **14**(7), 1393–1411 (1997).
28. N. Johnson, S. Kotz, and N. Balakrishnan, *Continuous Univariate Distributions, Volume 1*, Wiley Series in Probability and Statistics (Wiley, 1994).
29. L. C. Andrews, *Special Functions of Mathematics for Engineers*, Volume 49 of SPIE Press monograph (SPIE Press, 1998).
30. D. A. Rowlands and G. D. Finlayson, "Mondrian representation of real world image statistics," in *Proc. London Imaging Meeting*, (2023), pp. 45–49.
31. B. N. Mukherjee and S. S. Maiti, "On some properties of positive definite Toeplitz matrices and their possible applications," Linear Algebra and its Applications **102**, 211–240 (1988).
32. M. Dow, "Explicit inverses of Toeplitz and associated matrices," ANZIAM J. **44**, 185 (2008).
33. L. T. Maloney, "Evaluation of linear models of surface spectral reflectance with small numbers of parameters," J. Opt. Soc. Am. A **3**(10), 1673–1683 (1986).
34. J. Jiang, D. Liu, J. Gu, *et al.*, "What is the space of spectral sensitivity functions for digital color cameras?" in *IEEE Workshop on the Applications of Computer Vision (WACV)*, (2013), pp. 168–179.